ORNL/CP-97102

57

Predictive Mathematical Modeling of Trickling Bed Biofilters for Elucidating Mass Transfer and Kinetic Effects

98-A955

CONF-980632--

John W. Barton

Chemical Engineer, Oak Ridge National Laboratory

X. Shaw Zhang

Chemical Engineer, Oak Ridge National Laboratory

K. Thomas Klasson

Remediation Technology Group Leader, Oak Ridge National Laboratory

Brian H. Davison

Biochemical Engineering Group Leader, Oak Ridge National Laboratory

ABSTRACT

Mathematical models of varying complexity have been proposed in the open literature for describing uptake of volatile organics in trickling bed biofilters. Many simpler descriptions yield relatively accurate solutions, but are limited as predictive tools by numerous assumptions which decrease the utility of the model. Trickle bed operation on the boundary between mass transfer and kinetic limitation regimes serves as one example in which these models may be insufficient One-dimensional models may also fail to consider important effects/relationships in multiple directions, limiting their usefulness.

This paper discusses the use of a predictive, two-dimensional mathematical model to describe microbial uptake, diffusion through a biofilm, and mass transfer of VOCs from gas to liquid. The model is validated by experimental data collected from operating trickle-bed bioreactors designed for removing sparingly soluble gaseous contaminants. Axial and radial (biofilm) concentration profiles are presented, along with validation results. Operation in regimes in which both mass transfer and kinetic factors play significant roles are discussed, along with predictive modeling implications.

INTRODUCTION

Although biofiltration of volatile organic contaminants (VOCs) has received much attention in the past decade,[1,2,3,4,5] several challenges associated with this process make optimization difficult. First, rates of removal are much slower than incineration or adsorption. Second, bacteria grow in an aqueous environment, and some VOCs are only sparingly soluble in water; difficulty thus arises in transferring gases into the aqueous phase. To address these problems, improved bioreactor designs are required which have a high active biocatalyst concentration and efficient mass transfer of the VOC from air to the liquid medium. Optimization necessitates a better understanding of the mechanisms by which biofilters function and can be approached through modeling and maximizing appropriate conditions for removal.

DISCLAIMER

Although predictive mathematical models have been available for a wide variety of biological systems, development and verification studies of models for trickle-bed bioreactors remain sparse in the literature. Shareefdeen and Baltzis[6], assuming mass-transfer limitation, successfully applied a steady state model to a peat/perlite biofilter constructed to remove toluene. Diks and Ottengraf[7], assuming negligible mass-transfer limitation for a sparingly soluble gas, successfully applied a model for removal of dichloromethane from waste gases in a biofilter based on zero-order biological uptake. Little consideration has been given thus far as to how the possible operating regimes associated with the processes of mass transfer and biological removal can be identified during bioreactor operation. Furthermore, the extent to which each plays a role in biofiltration is further clouded by the difficulty in measurement of the necessary parameters required to incorporate both processes into a successful mathematical model.

A number of bioreactor types can be used for VOC treatment. Gas-continuous trickle-bed reactors, used in this study, contained structured plastic packing on which a thin film of bacteria grew. A nutrient mineral solution (containing available nitrogen, phosphorus, and other mineral nutrients) was distributed from a source at the top of the reactors to keep the packing moist and nutrient-rich as desired. VOCs entered at one end of the column, and were degraded as they passed through and over the packing. These bioreactors provided a high surface area for gas-liquid contact and incurred low operating costs due to a minimal amount of pumping necessary to run the reactors. Additionally, the external source of supplemental nutrients controlled the growth of bacteria such that the reactor required very little maintenance. The trickle-bed bioreactor system was mathematically modeled to learn more about the parameters affecting removal and to determine if consumption of VOCs in the reactor was kinetically limited, mass transfer limited, or both. A more detailed description of these trickle beds has been published previously[9].

METHODOLOGY

Problem Formulation. The system is a symmetric trickle-bed bioreactor of fixed biofilm thickness, $\delta_b = x_2 - x_1$, with a liquid film having thickness, δ_1, and gas surrounding it, as shown in Figure 1. It is convenient to define rectangular coordinates (x, z), whose origin lies at the top of the interface between the liquid film and gas phase, also shown in Figure 1. As substrate (VOC) enters the system (as a component of the gaseous inlet stream) with concentration C_0 (mole/cm^3), it transfers into the liquid by diffusion and convection. Then it transfers into the biofilm (also in the x-direction) by diffusion due to the concentration gradient and is removed by the biomass.

Diffusion-convection-reaction equations can be derived[8] to describe the steady-state mass transfer process in gas, liquid, and biomass phases, respectively, with assumptions that the substrate flux in the x direction due to convection is negligible compared with that by diffusion and the reaction follows simple Monod kinetics.

Equation 1.

$$V_z^g \frac{\partial C}{\partial z} - D\frac{\partial^2 C}{\partial x^2} = 0$$

for $x_3 \leq x \leq 0$

Equation 2.

$$V_z^l \frac{\partial C}{\partial z} - D\frac{\partial^2 C}{\partial x^2} + X_l q_m \frac{C}{K_s + C} = 0$$

for $0 \le x \le x_1$

Equation 3.

$$-D\frac{\partial^2 C}{\partial z^2} - D\frac{\partial^2 C}{\partial x^2} + X_b q_m \frac{C}{K_s + C} = 0$$

for $x_1 \le x \le x_2$

With boundary conditions

Equation 4.

$$C(x = 0, z) = C_0^l$$

for $0 < z < L$

Equation 5.

$$C(x, z = 0) = 0$$

for $0 < x \le x_2$

Equation 6.

$$C(x, z = 0) = C_0^g$$

for $x_3 < x \le 0$

Equation 7.

$$\frac{\partial(x,0)}{\partial x} = 0$$

for $0 < z < L$

Where $V_z(x)$ is the velocity profile, C is molar concentration of the substrate, D is the diffusivity, X_i is the biomass density (i = 1 and b for the liquid and biomass phases, respectively), q_m is the maximum specific uptake rate, and K_s is the Monod saturation constant.

Solving these second-order, nonlinear partial differential equations, though well-defined and solvable numerically, is a challenge and involves complex numerical calculations. In practical operations of trickle-bed bioreactors, it is assumed that, within the very thin liquid film and biofilm, substrate transfer in the z direction can be negligible compared to that in the x direction due to the large diffusion and reaction rate and stagnant biofilm. Estimates show that the ratio of substrate transfer rates in the x direction by diffusion ($D\,\partial C/\partial x$) and z direction by convection (Cv_z) to be $\sim 10^5$ at the conditions of the liquid flow rate of 10 cm^3/min ($V_z \sim 0.02$ cm/s) and $\partial C/$

$\partial x \sim 2$ mol/cm^4 (which is determined by numerical model). It is also assumed that the gas is well mixed and, therefore, the substrate concentration can be treated as the sum of a diffusion contribution and a bulk gas flow contribution. An effective mass transfer coefficient, $K_l a$, may be defined to describe the process[9]. For the processes at which the concentrations of substrate are always small (< 5000 ppm in the gas phase), transfer may be considered isothermal and the mass transfer coefficient, $K_l a$, need not be corrected for mass transfer rate along the reactor column[10]. Therefore, for simplification, the 2-D mass transfer problem, which is described by Equations (1) – (3), may be decomposed into two directions and solved separately for the distributions of substrate concentration in the x direction within the liquid film and biofilm and in the z direction within gas phase. An effectiveness factor, η, must also be incorporated into the model to account for diffusional resistance within the biofilm.

Finite Element Analysis. Mass flux of substrate through the liquid film ($0 < x < x_1$) and biofilm ($x_1 < x < x_2$) at a certain, arbitrary location along the axis of a bioreactor, z, is given by[8]

Equation 8.

$$N_x = -\frac{D}{1-f_x}\frac{\partial C}{\partial x}$$

Balancing the mass flux and reaction and assuming the mole fraction of substrate, f_x, is much less than unity yields

Equation 9.

$$-D\frac{\partial^2 C}{\partial x^2} + X_i q_m \frac{C}{K_s + C} = 0$$

Equation (9) is non-dimensionalized using C_0 as the mole density scale and x_2 as the length scale and then the governing system for substrate concentration within liquid film and biofilm is given by:

Equation 10.

$$\frac{\partial^2 C}{\partial x^2} - \Phi_i^{\,2}\frac{C}{1+\beta C} = 0$$

Where

Equation 11.

$$\Phi_i = x_2\sqrt{\frac{X_i q_m}{DK_s}}$$

And

Equation 12.

$$\beta = \frac{C_o}{K_s}$$

With boundary conditions

Equation 13.

$$\frac{\partial C}{\partial x}(1) = 0$$

Equation 14.

$$C(0) = 1$$

Where Φ_i is the Damkohler number (i = b and 1, for biofilm and liquid film, respectively), which measures the relative importance of the reaction rate and diffusion rate, and β is the dimensionless initial mole density. Note, from now on, c and x represent non-dimensional components. This diffusion-reaction equation is solved subject to the boundary conditions that dimensionless mole density in the liquid phase at the interface (x = 0) is equal to unity and the derivation of dimensionless mole density, c, with respect to x vanishes at the center line (x = 1) due to symmetry.

The governing nonlinear Equations (10,11,12) were solved numerically in this work by the Galerkin/finite element method. The numerical procedure is standard and the details can be found elsewhere.[10,11] The domain, $0 \le x \le 1$, is divided into NE elements. The unknown, c, is then expanded in terms of series linear basis functions $\phi^i(x)$:

Equation 15.

$$c(x) = \sum_{1}^{N} c_i \phi^i(x)$$

where c_i is the unknown coefficient to be determined and N=NE+1.

The Galerkin weighted residual of Equation (10) is constructed by weighting the equation by the basis function and integrating the resulting expression over the computational domain. The weighted residuals of Equation (10) are next integrated by parts to reduce the order of the highest-order derivative appearing in it and the resulting expression is then simplified because of boundary conditions. With these manipulations, the residual equation becomes:

Equation 16.

$$R_i = \int_0^1 \left(\frac{\partial \phi^i}{\partial x}\frac{\partial c}{\partial x} - \frac{\Phi_i^2 c}{1+\beta c}\phi^i\right)\partial x = 0$$

The Galerkin weighted residual (10) is integrated by Gaussian quadrature. The resultant nonlinear algebraic equations are then solved by Newton's method: given an initial approximation $c^{(0)}$ to the solution, the $(k+1)^{th}$ approximation is obtained from the k^{th} value by

Equation 17.

$$\underline{\underline{J}}(c^k)\cdot(\underline{c}^{(k+1)} - \underline{c}^{(k)}) = -\underline{R}(c^{(k)})$$

Where

$\underline{\underline{J}}$

is a Jacobian matrix of partial derivatives, given by:

Equation 18.

$$J_{ij} = \frac{\partial R_i}{\partial c_j} = -\int_0^1 [\frac{\partial \phi^i}{\partial c}\frac{\partial \phi^j}{\partial x} - \frac{\Phi_i^2 \phi^i \phi^j}{(1+\beta c)^2}]\partial x$$

The linear system that results at each Newton iteration is then solved by direct factorization with a Hood's frontal solver.[12] The Newton iteration is continued until the Euclidean norm, i.e., the square root of the sum of squares, of both solution update $\Delta c^{(k+1)}$ and residual $R^{(k)}$ are less than a prescribed tolerance.

Computer Program. The algorithm for calculating the substrate concentration (or mole density, c_i) has been programmed in FORTRAN and Microsoft Visual BASIC. The FORTRAN program is written as separated subroutines for different functions. Clarity is emphasized in the programming, with necessary lines being comments and definitions to aid the user. Microsoft Visual BASIC code is compiled into a 32-bit program which runs in Windows 95/98 environments in the absence of external software packages. This particular type of coding is particularly useful, not only because of a user-friendly graphical interface, but also because it can be run on most IBM-compatible computers.

Effectiveness Factors. Typically in trickle-bed systems, the only experimentally measurable values are those for bulk phase (gas) concentrations. The kinetic model used in this simulation employs bulk concentrations. Because of this, an effectiveness factor is incorporated into the model to account for the effect of diffusion on the reaction rate and correct for the fact that the actual concentration is different from the bulk. The effectiveness factor is defined as the ratio of actual reaction rate per unit biomass to the rate which would result if the complete internal depth of the biocatalyst were available for the reaction. An alternative expression for the effectiveness factor, η, is

Equation 19.

$$\eta = \frac{\int_0^{x_2} \frac{C_l(x)}{1+\beta C_l(x)} dx}{\frac{C_l(x_1)}{1+\beta C_l(x_1)}}$$

When the computer program solves the biocatalyst mathematical model equations, it also generates effectiveness values which are then used to calculate z-direction model values. The effectiveness factors are somewhat dependent upon z, which is taken into account by generating

factors for different axial positions as the equations are solved. These values generally vary from about 0.21 to 0.23 across the length of the column for the experimental conditions described.

RESULTS AND DISCUSSION

The effects of important operation parameters - film thickness, δ_i, the biomass density, X_i, and initial concentration C_0- were studied quantitatively by systematically varying one of these variables while maintaining all others. Variation of the parameters was confined within reasonable operating ranges. The calculated concentration as a function of distance, x, within the films are presented in dimensionless forms for generality. In particular, the calculated dimensionless concentration (or mole density) of substrate can be used at different locations along the axis of a bioreactor column (in the z direction) where the initial concentration, C_0, is different (see below).

Figure 2 shows computational prediction of the substrate concentration (mole density), c, within a biofilm with a vanishing liquid film at different biomass densities of the biofilm, X_b. The results show that the substrate concentration decreases with penetration depth due to microbial uptake. The biomass density significantly affects the mechanism of substrate transfer in terms of the distribution of substrate concentration within the film. Apparently, for low biomass density, the concentration decreases slowly as a result of the small reaction rate, indicating the process to be kinetically limited. In contrast, the larger biomass density causes faster reaction, yielding the result that the substrate concentration in the biofilm decreases with a larger slope. In this latter case of larger biomass density, mass transfer across the interface is the dominant effect on biofiltration. Obviously, at actual experimental conditions, the results of which are shown as the central, solid line in Figure 2, both kinetic and mass transfer are important factors to be considered.

Similar features of the substrate concentration varying with x are also seen at different film thickness, δ_b, as shown in Figure 3. Simulations such as those shown in Figures 2 and 3 may be used to predict optimal biomass density and film thickness.

Figure 4 shows the effects of initial substrate concentration, C_0, on concentration distribution within the biofilm. Dimensionless concentration in the biofilm is a weak function of the initial concentration since the Monod saturation value (a function of microbial kinetics) is always larger than aqueous phase substrate concentrations. However, it is noteworthy that the dimensional concentration differs considerably in its magnitude following the difference in its initial concentration, while the change rate of the concentration with x (or the slope) remains steady. Another way of expressing this is that the reaction rate order (first order in this case) is independent of substrate concentration.

The effects of a surrounding liquid film on biofiltration is shown in Figure 5 for different film thicknesses, δ_l. In the calculations for results in Figure 5, the mole densities of substrate on either side of the interface between the liquid film and biofilm are set to be equal due to the continuity. In Figure 5, the origin of the x axis is manually moved to the top of the interface between the liquid film and biofilm to distinguish the liquid film and to keep the biofilm fixed in position. Although thicker liquid films result in lower substrate concentrations at the entrance of the biofilm, concentration distribution within the biofilm changes relatively little. This computational result indicates that thin liquid films play an insignificant role on mass transfer of

substrate in the trickle-bed bioreactor for the gases used in these experiments.

As a test of accuracy and validation of the finite element analysis, numerical results were compared with analytical results for the case of $C << K_s$, where first order reaction occurs. The diffusion-reaction equation becomes linear:

Equation 20.

$$\frac{\partial^2 c}{\partial x^2} - \Phi_i^2 c = 0$$

with boundary conditions

Equation 21.

$$c(0) = 1$$

Equation 22.

$$\frac{\partial c(1)}{\partial x} = 0$$

Integrating this linear homogenous differential equation analytically yields a closed form of the solution:

Equation 23.

$$c = \frac{1}{1+e^{2\Phi_i}} e^{\Phi_i x} + \frac{1}{1+e^{2\Phi_i}} e^{-\Phi_i x}$$

The comparison of numerical and analytical solutions at $\beta = C_0/K_s = 0.0373$ (data not shown) revealed that both solutions are in good agreement within most of the biofilm.

MASS TRANSFER ALONG BIOREACTOR COLUMN

Mathematical description of distribution of substrate concentration along a bioreactor column (in the z direction) has been accomplished by setting up a mass balance around a subsection of the column.[13] For consistency of the nomenclature, the available governing equations are converted for mole density and non-dimensionalized, yielding

Equation 24.

$$\frac{\partial c^g}{\partial z} = -L\frac{K_l a}{H}(c^g - c^l)\frac{SRT}{G}$$

Equation 25.

$$\frac{\partial c^l}{\partial z} = -L\frac{S}{Q}[K_l a(c^g - c^l) - \eta\frac{X_l q_m}{K_s}\frac{c^l}{1+\beta c^l}]$$

With boundary conditions

Equation 26.

$c^g(0) = 1$
Equation 27.

$c^l(0) = 0$

where L is the length of the column, S is the area of the cross section, H is Henry's law coefficient, R is the gas constant, T is the absolute temperature, G is the gas flow rate, Q is the liquid flow rate, and η is the effectiveness factor. The equations are non-dimensionalized with the concentration scale, C_0^g of initial concentration in gas phase, and length scale, L. Numerical solutions for the governing Equations (23, 24) were obtained by using finite element techniques programmed in FORTRAN and Visual BASIC. One-dimensional solutions were verified by comparing solutions with finite difference techniques available in MathCAD 7.0 Professional for Windows.

A typical solution of concentration distribution in gas and liquid phase along the reactor column is shown in Figure 6 using parameters from actual experimental conditions. It accords with intuition that the substrate concentration decreases along the column due to its transfer into and reaction within the biofilm. At this condition, unreacted substrate exits the column and removal is incomplete. Figure 7 shows the effect of gas flow rate on distribution of substrate concentration along the reactor column in gas phase. It is apparent that with lower gas flow rate, substrate has more time to transfer into the biofilm and react with biomass, resulting in less substrate leaving the reactor. Optimal conditions may be achieved by balancing competing effects.

Consistent with predictions that the effects of liquid film characteristics are minimal on biofiltration, liquid flow rate, Q, did not affect the process significantly (see Figure 8) and the results for the concentration distribution at different liquid rates overlap at most of the column.

EVALUATION OF BIOFILTRATION BY TRICKLE BED BIOREACTOR

Since effects of the liquid film are minimal, as predicted by above models, the liquid film can then be assumed to be infinitely thin and the substrate concentration in the liquid film to be constant (across the film thickness). The predicted concentrations in liquid phase at different locations (z) along the column are treated as boundary conditions at x = 0 for the model solving the diffusion reaction equation to determine the biofiltration feature in the entire reactor column in terms of the concentration. Figure 9 shows calculated results for the concentration distribution within the biofilm at different axial positions when the gas flow rate is held constant. Results predict that different mechanisms of biofiltration may occur at different locations along the reactor. In particular, at the lower gas flow rates, substrate levels within the biofilm decrease significantly as gas moves towards the bottom of the reactor, indicating a conversion from mass transfer limitation to kinetics limitation. In these cases, the assumption of constant effective mass transfer coefficient may no longer be valid.

The model can successfully estimate outlet concentrations and axial profiles based on parameters determined independently (no fitted parameters) such as the specfic uptake constant and Monod saturation constant. In Figure 10, experimental data collected from a trickle bed are compared with model predictions. In one case, the reactor was operated at 30°C with an inlet VOC

concentration of 500 ppm isobutane. In the other case shown, n-pentane was used (500 ppm) and the temperature was lowered to 15°C. In both cases, the model closely predicts the actual outlet concentration for a wide range of gaseous flow rates, although there is uniform underprediction of total removal. Small adjustments in certain parameters, such as the specific uptake rate or Henry's law constant, play an important role in determining closeness of fit. It is likely that biomass uptake rates for the biofilm are different from the dispersed biomass in batch vessels, from with kinetic data were collected. In addition, Henry's law coefficients in moist biomass are likely to be different than those measured for pure water. We have used the best available values to compensate for this effect, and are investigating how these changes can affect biofilter performance.

CONCLUDING REMARKS

Theoretical/numerical models in two dimensions have been developed to predict the distribution of substrate concentration throughout bioreactor columns. The resulting calculations alllowed a more exhaustive exploration of parameter space for optimization of operation conditions.

Although the model developed is based on sophisticated algorithms and sound simplifications, some assumptions may not be valid for certain operations. Even so, the two-dimensional solution has led to better and more accurate predictions of biofiltration of operating trickle-bed reactors based upon independently measured parameters. Further comparison of the numerical results and experimental measurements will enhance the accuracy and disclose the range of validity of the theoretical/numerical model.

ACKNOWLEDGMENTS

The authors gratefully acknowledge the U.S. Department of Energy Environmental Management Science Program for sponsoring this research.

REFERENCES

1. Andrews, G. F., Noah, K. S. Design of Gas-treatment Bioreactors. *Biotech. Prog.* 1995, 11, 498-509.
2. Davison, B. H., Thompson, J. E. Sustained Degradation of n-pentane and Isobutane in a Gas phase Bioreactor. *Biotech. Lttrs.* 1993, 15, 633-636.
3. Davison, B. H., Thompson, J. E. The Removal of Alkanes in a Liquid-Continuous Gas-Phase Bioreactor: Preliminary Considerations. *Appl. Biochem. Biotech.* 1994, 45/46, 917-923.
4. Klasson, K. T., Cowger, J. P., Ko, C. W., Vega, D. L., Clausen, E. C., Gaddy, J. L. Methane Production from Synthesis Gas Using a Mixed Culture of *R. rubrum*, *M. barkeri*, and *M. formicicum*. *Appl. Biochem. Biotech.* 1990, 24/25, 317-328.
5. Leson, G., Winer, A. M. Biofiltration: An Innovative Air Pollution Control Technology for VOC Emissions. *J. Air Waste Mgm. Asssoc.* 1991, 41, 1045-1054.
6. Shareefdeen, Z., Baltzis, B. C. Biofiltration of Toluene Vapor Under Steady-State and Transient Conditions: Theory and Experimental Results. *Chem. Eng. Sci.* 1994, 49, 4347-4360.

7. Diks, R. M. M., Ottengraf, S. P. P. Verification Studies of a Simplified Model for the Removal of Dichloromethane from Waste Gases Using a Biological Trickling Filter (Part I). *Bioprocess Eng.* 1991, 6, 93-99.

8. Bird, R.B., Stewart, W.E., Lightfoot, E.N. *Transport Phenomena,* John Wiley & Son, New York 1960.

9. Barton, J.W., Klasson, K.T., Koran, L.J. and Davison, B.H. Microbial Removal of Alkanes from Dilute Gaseous Waste Streams, *Biotech. Prog.* 1997, 13, 814-821.

10. Strang, G, Fix, G.J. *An Analysis of the Finite Element Method.* Prentice-Hall, 1973.

11. Zhang, X.; Padgett, R. S.; Basaran, O.A. Nonlinear Deformation and Breakup of Stretching Liquid Bridges, J *FluidMech.* 1996, 329, 207.

12. Hood, P. Frontal Solution Program for Unsymmetric Matrices. *mt. J Numer. Meth. Engng* 1976, 10, 379.

13. Cowger, *J. P.;* Klasson, K.T.; Ackerson, M.D.; Clausen, E.C.; Gaddy, J.L. Mass-Transfer and Kinetic Aspects in Continuous Bioreactors Using *Rhodospirillum rubrum, Appl Biochem Biotech.* 1992, 34/35, 613.

Figure 1. Two-dimensional geometry of trickle bed bioreactor used in formulating mathematical model.

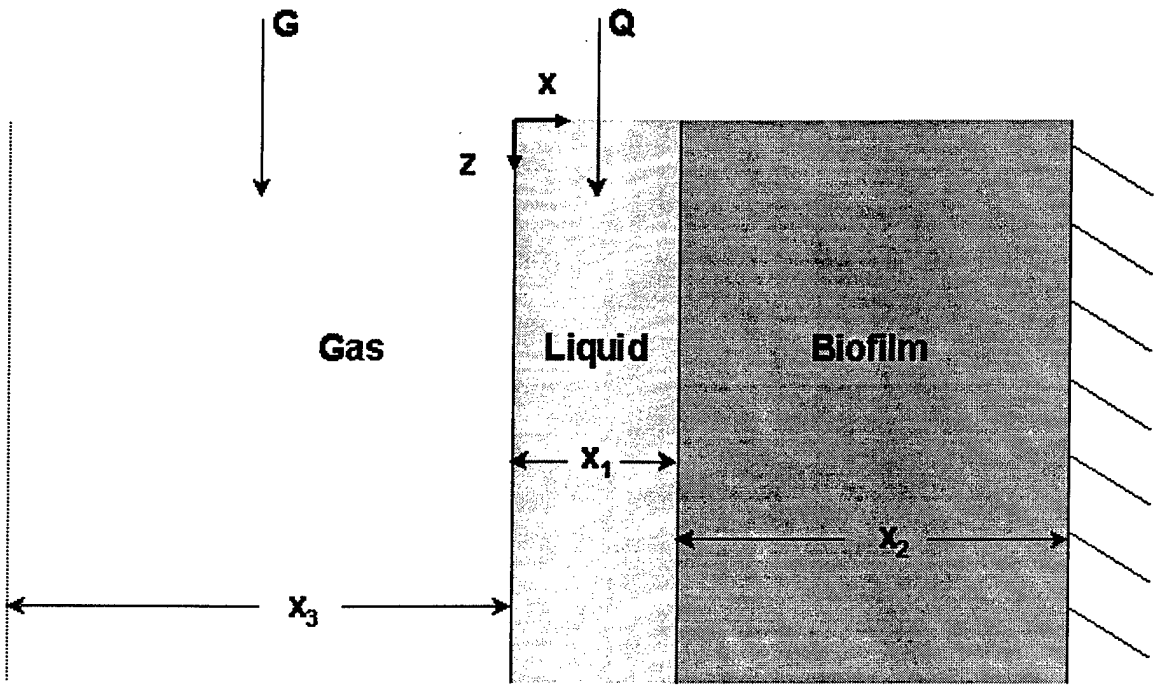

Figure 2. Predicted biofilm VOC concentration profiles for three biocatalyst densities (dry weight). The midline value corresponds to actual operating condition for the trickle beds used in experiments.

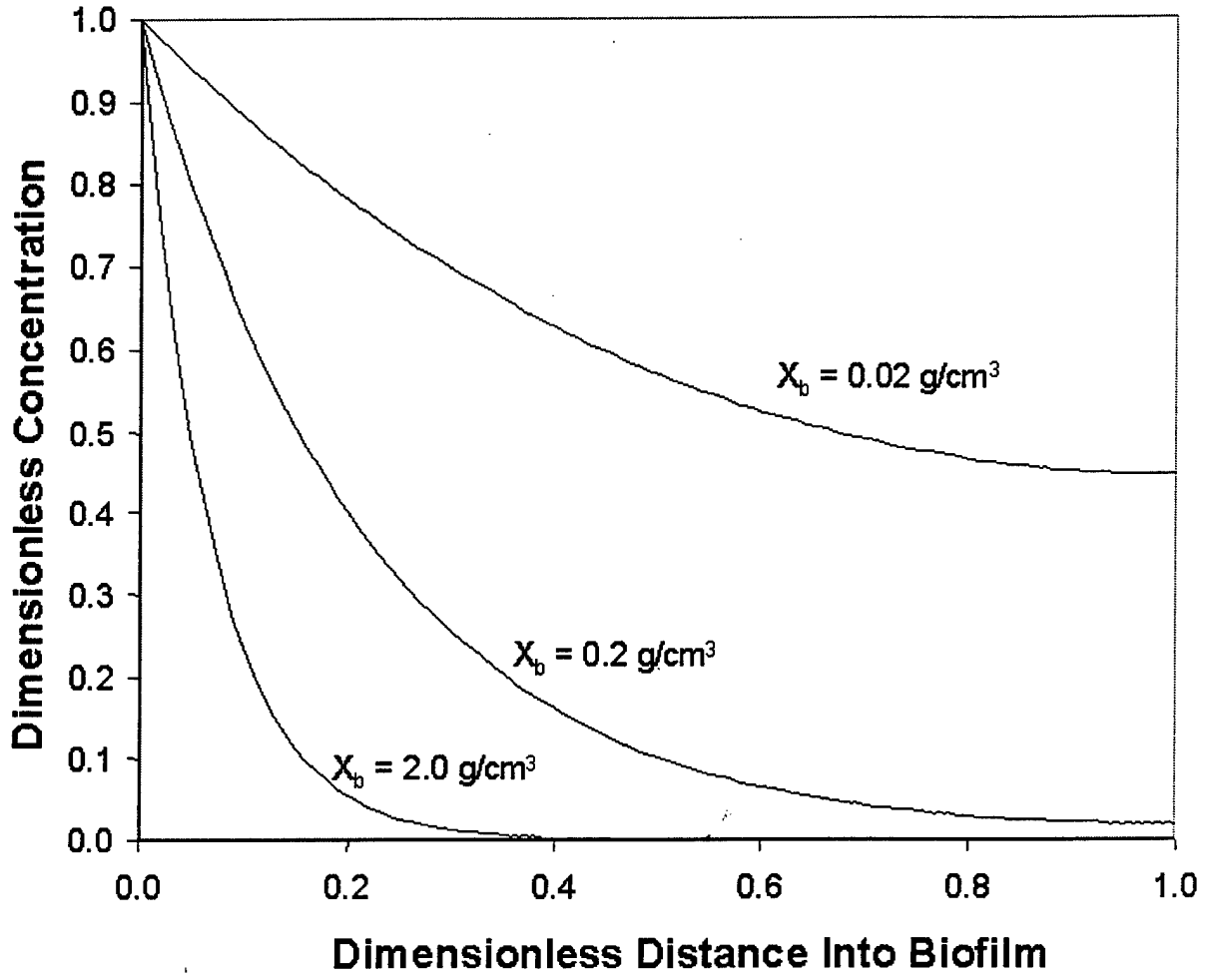

Figure 3. Predicted biofilm VOC concentration profiles for three biofilm thicknesses. The midline value corresponds to the actual value measured for the trickle beds used in this study.

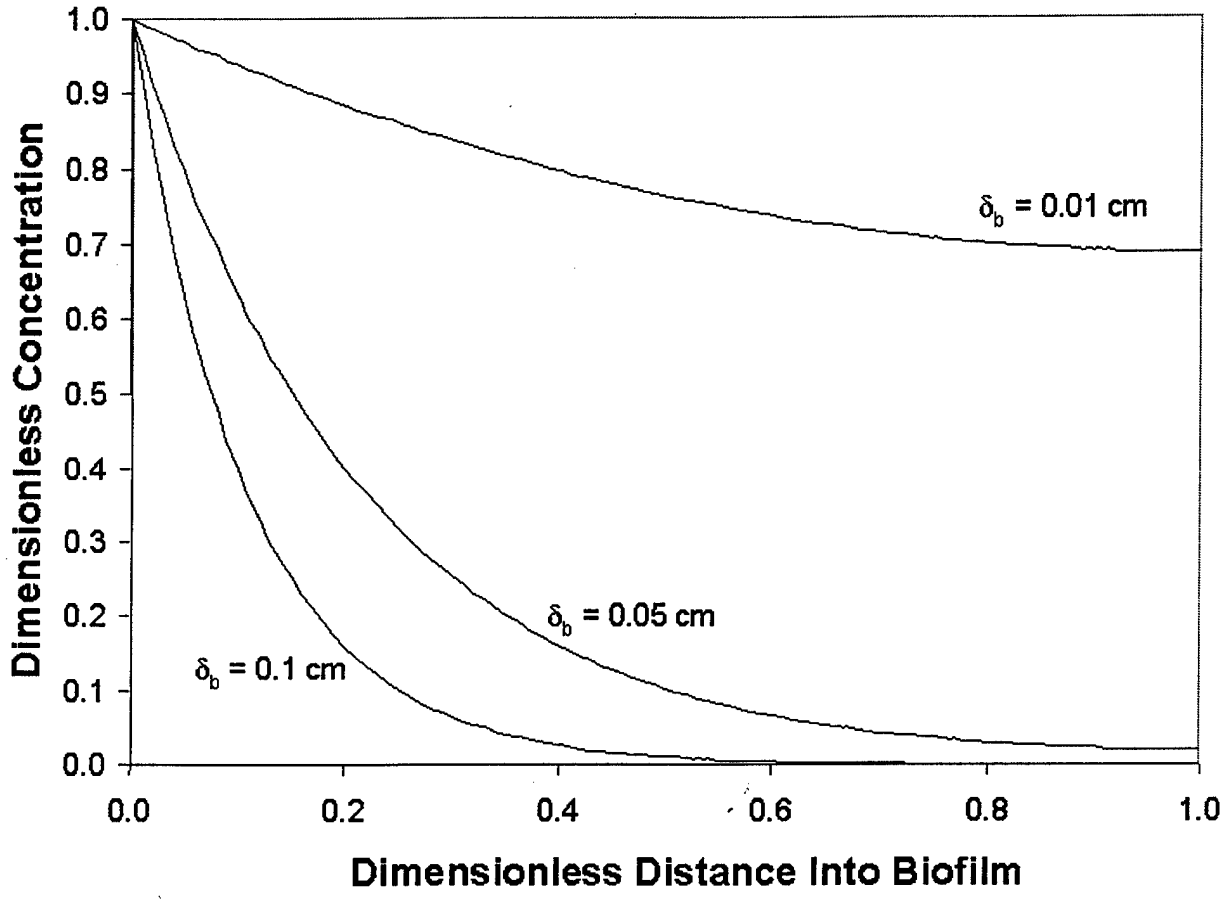

Figure 4. Predicted biofilm VOC concentration profiles (dimensionless) for three markedly different initial inlet concentration. This graph demonstrates that the shape (rate of change) of the profile remains constant with gas-phase substrate concentration. The actual concentration changes directly with the gas phase concentration (not shown).

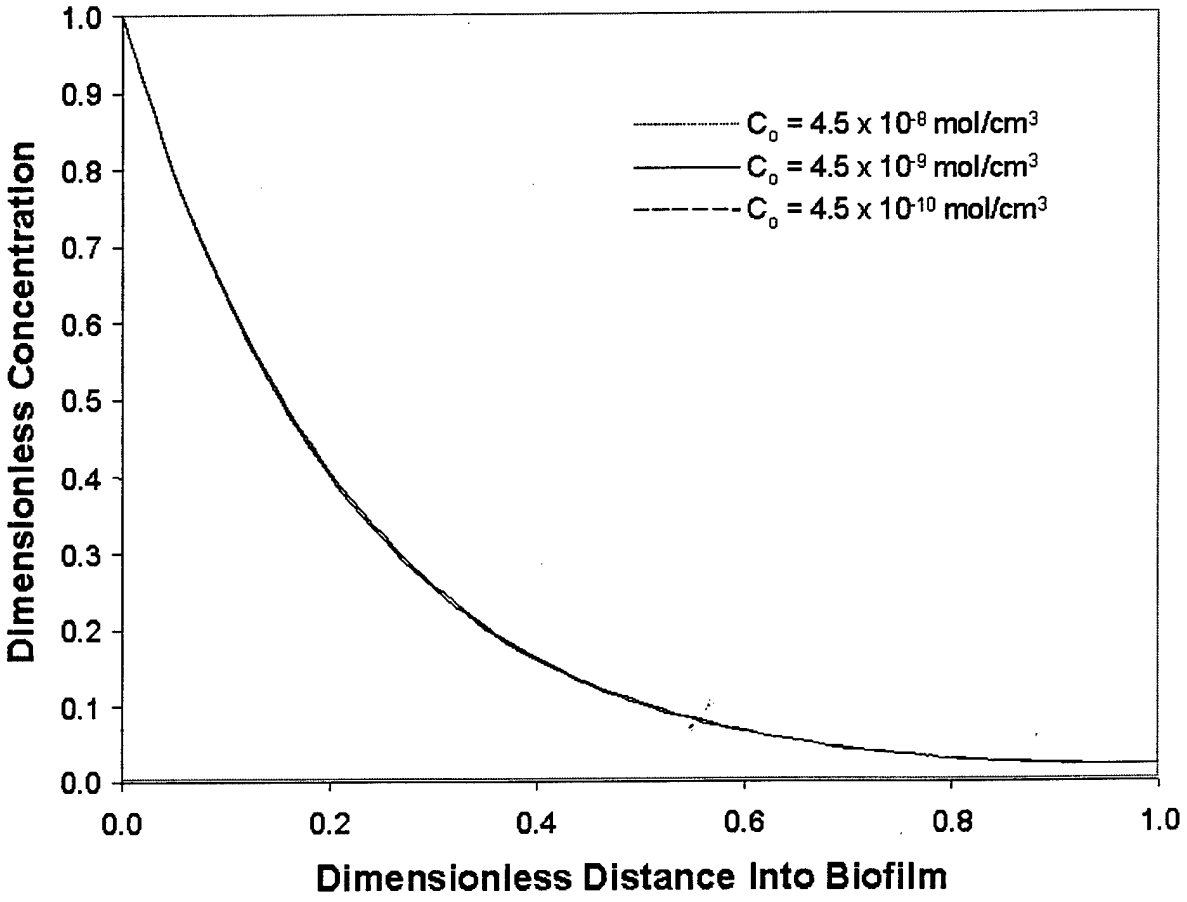

Figure 5. Predicted biofilm and liquid layer VOC profiles for three different liquid film thicknesses. In general, very little degradation occurs within the liquid film since the biocatalyst concentration is small. The model predicts that the effects due to the liquid film can be neglected in many cases.

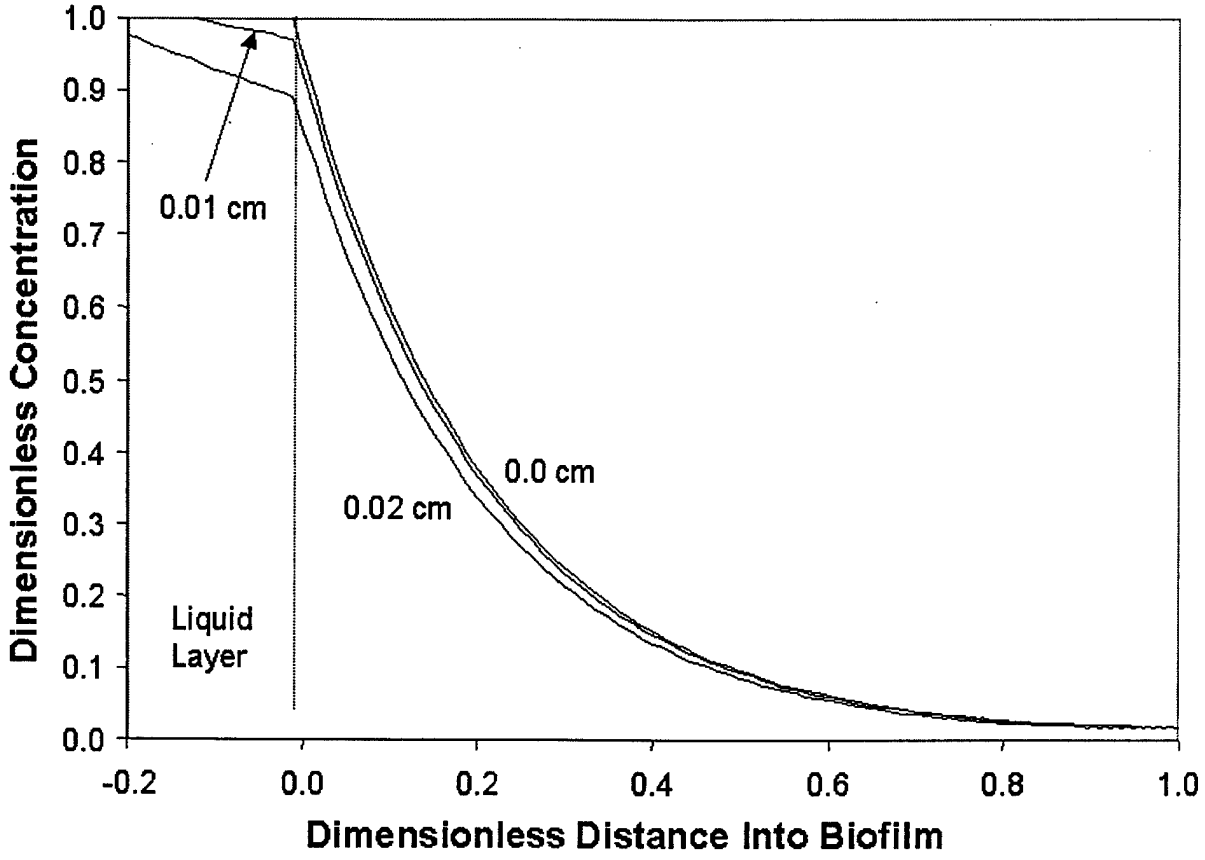

Figure 6. Predicted axial VOC concentration profiles in both the liquid and gas phases. Standard experimental operating parameters are used.

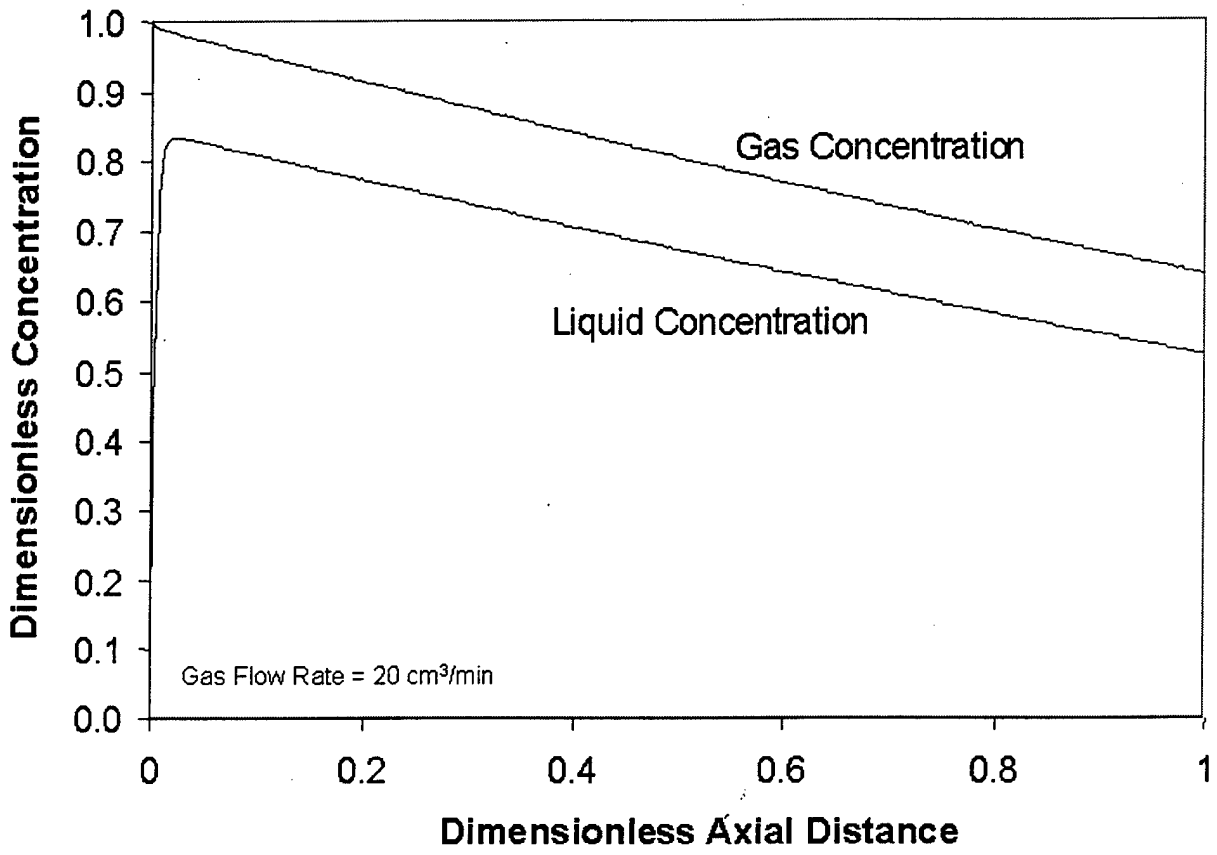

Figure 7. Predicted axial VOC concentration profiles (gas phase) for a variety of gas flow rates.

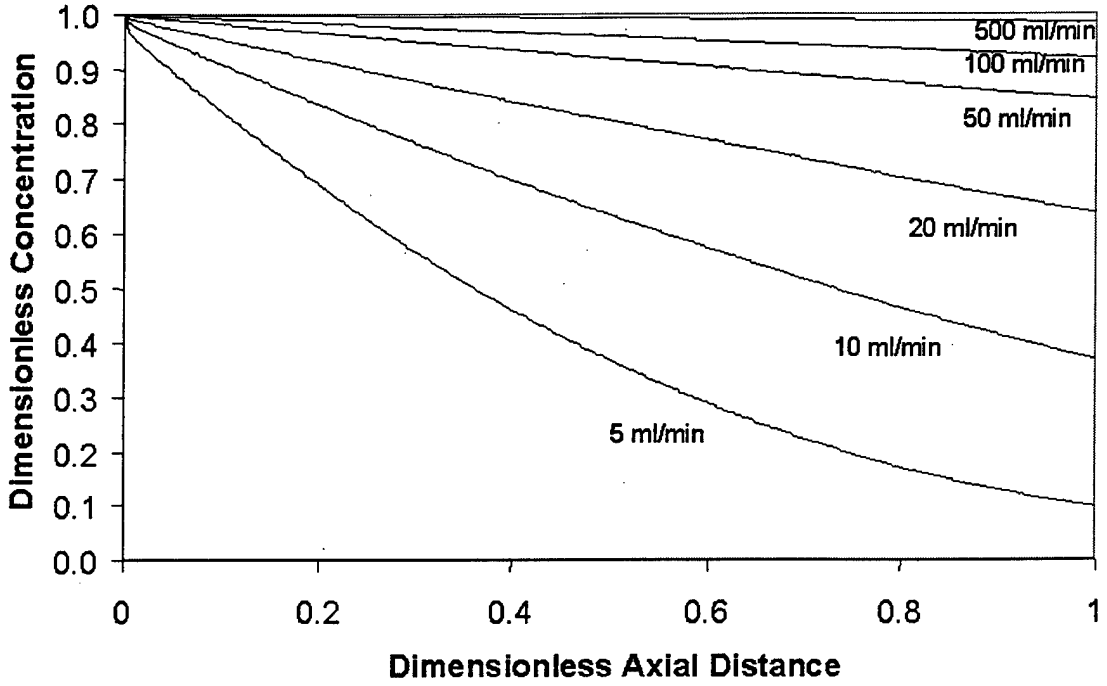

Figure 8. Predicted axial VOC concentration profiles (both liquid and gas phase) for three widely different values of the liquid flow rate. In general, the effect of the liquid flow rate on removal is negligible.

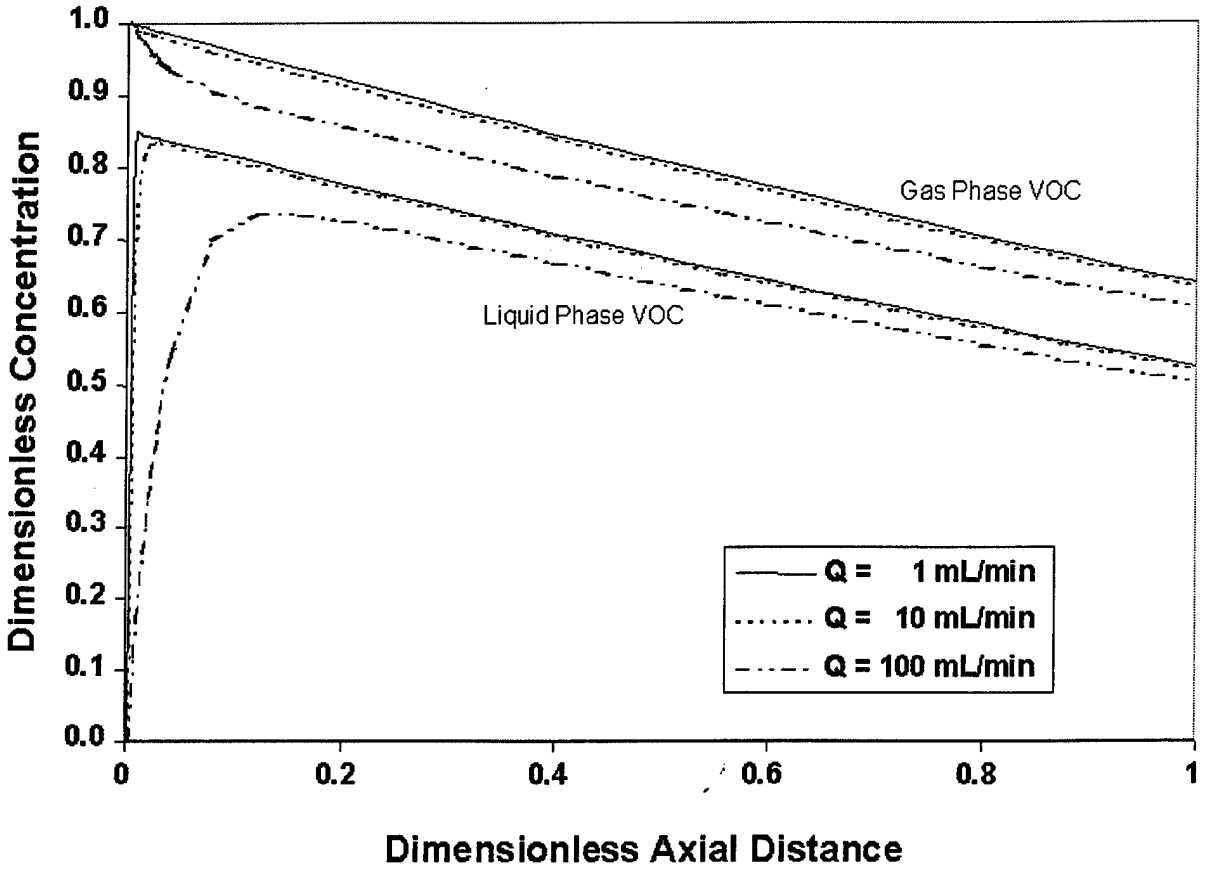

Figure 9. Predicted VOC concentrations in biofilm at different axial positions.

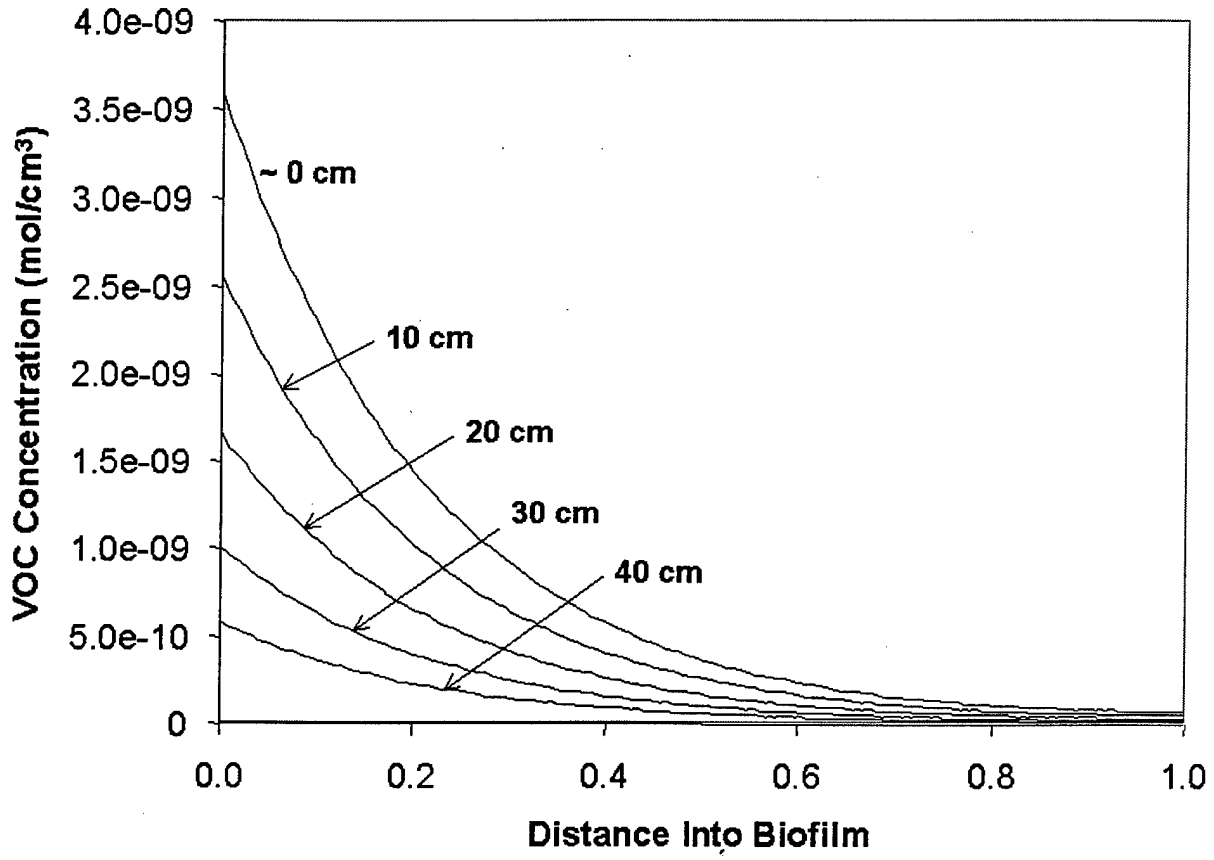

Figure 10. Comparison of experimentally obtained outlet concentrations with model predictions for two different cases. Inlet concentration in each case was 500 ppm isobutane or n-pentane. In general there is fairly good agreement, with some underprediction of total VOC removal. Parameters used in the model were measured independently (not fitted).

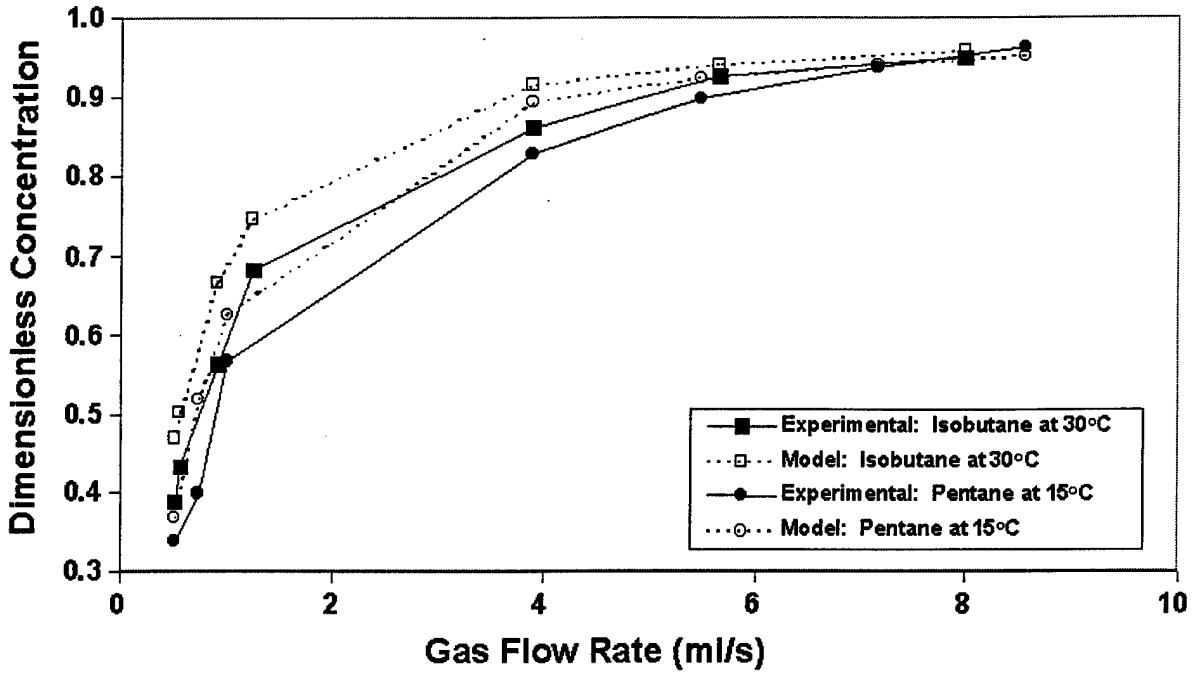

Report Number (14) ORNL/CP--97102
CONF-980632---

Publ. Date (11) 199803
Sponsor Code (18) DOE/EM, XF
UC Category (19) UC-2000, DOE/ER

DOE